IEEE Access
Multidisciplinary ⋮ Rapid Review ⋮ Open Access Journal

Received 13 April 2023, accepted 29 April 2023, date of publication 4 May 2023, date of current version 16 May 2023.

Digital Object Identifier 10.1109/ACCESS.2023.3272895

RESEARCH ARTICLE

Non-Contact Heart Rate Measurement Based on Adaptive Notch Filter and Elimination of Respiration Harmonics

MOUSHUMI TAZEN[1], (Student Member, IEEE), NAOTO SASAOKA[1], (Member, IEEE), AND YOSHIHARU OKAMOTO[2]

[1]Faculty of Engineering, Tottori University, Tottori 680-8552, Japan
[2]The Veterinary Advanced Medical Research Institute, Wolves Hand Company Ltd., Osaka 550-0015, Japan

Corresponding author: Moushumi Tazen (d21t2002u@edu.tottori-u.ac.jp)

This work was supported by JSPS KAKENHI under Grant JP21K04094.

ABSTRACT Continuous-wave Doppler radar is an established method for non-contact heart rate estimation. The output signal of the Doppler radar includes the fundamental wave of a heartbeat, heartbeat harmonics, the fundamental wave of respiration, respiration harmonics, and artifacts due to body movement. The respiration harmonics and artifacts degrade the accuracy of heart rate estimation. To this end, a novel heart rate estimation method is proposed that uses adaptive notch filters (ANFs). First, the proposed system estimates respiration frequency. Next, cascaded notch filters, the notch frequencies of which are controlled by the estimated respiration frequency, eliminate respiration harmonics; thus, the accuracy of heart rate estimation improves. In addition, the proposed method uses an ANF based on all-pass filter and an adaptive algorithm to estimate heart rate. The ANF is robust against disturbances, allowing the proposed method to improve the estimation accuracy in the presence of moving artifacts. The simulation results for human subjects show that MAPE, MAE, MSE, and RMSE of the proposed method are 5.24%, 4.00, 28.38, and 5.26, respectively; thus, they can be reduced up to fourth-order respiration harmonics. In an experiment on a dog not restrained in a cage, the proposed method, handling up to the fifth-order respiration harmonic, yields MAPE of 7.89%, MAE of 5.34, MSE of 96.11, and RMSE of 9.80. Thus, the proposed method shows better estimation accuracy than any other conventional method.

INDEX TERMS 24-GHz continuous-wave Doppler radar, non-contact vital monitoring, adaptive digital filter.

I. INTRODUCTION

Non-contact heart rate estimation is effective because it allows long-term monitoring without needing to attach uncomfortable sensors to body. Therefore, heartbeat and respiration rate detection systems using a Doppler radar have been attracting attention as they can collect biometric information in a non-contact manner. In recent years, animals are increasingly being treated as family members, and the expectations for their health care and management are correspondingly high. However, animals cannot communicate their health needs to humans; moreover, attaching contact sensors, such as an electrocardiogram (ECG), to exhausted animals causes discomfort and adds additional burden on veterinarians. Consequently, the use of non-contact sensors on animals has attracted increased research interest. Periodic and minute vibrations associated with breathing and heartbeat are prevalent on body surface. These minute vibrations can be detected using a Doppler radar and monitored by estimating respiration and heartbeat rates [1]. Juan et al. attempted to measure the respiration rate of a rat using a Doppler radar [2].

In addition to Doppler radar, Garbey et al. used thermal imaging for non-contact measurement in humans [3]. This method is based on the property that superficial vessels radiate thermal signals, and their temperature changes with blood flow. Parnandi et al. proposed using an eye tracker to measure

The associate editor coordinating the review of this manuscript and approving it for publication was Santosh Kumar.

heart rate from pupillary fluctuations [4]. This method takes advantage of the fact that pupillary and heart-rate fluctuations are under the control of the autonomic nervous system. Photoplethysmography (PPG)-based methods were also proposed to utilize the human face information obtained through a camera [5], [6], [7], [8]. They can detect the heartbeat from the green channel fluctuations because it features most characteristics of plethysmographic signals corresponding to hemoglobin absorption. A method using HSV, a color space different from RGB, has also been proposed [9]. Another technique uses face images obtained from visible and infrared videos [10]. Unfortunately, conventional methods [3], [4], [5], [6], [7], [8], [9], [10] use videos of human faces or pupils, rendering them difficult to apply on animals because animals' skin is not visible because their bodies, including their faces, are covered with hair, and pupil detection requires restraint of the animal. Therefore, in this study, we focused on the Doppler radar-based method.

Many systems have been proposed for heart-rate measurement using a continuous-wave Doppler radar, which is simple and low-cost. Droitcour developed a heart rate estimation system that involves peak search of autocorrelation or amplitude spectrum based on a fast Fourier transform (FFT) [1]. This system requires a long time window to maintain a high frequency resolution. Li et al. introduced the RELAX algorithm for parametric and cyclic optimization to estimate heartbeat and respiration frequency [11]. Tariq et al. developed a system that uses a continuous wavelet transform (CWT), which has a higher time-frequency resolution than FFT [12].

A received Doppler radar signal contains respiration and heartbeat components as well as moving artifacts and noise. Respiration harmonics in the frequency band of heartbeat component degrade the accuracy of heart rate estimation. Moving artifacts are generated by the body movement. An animal moves around in a cage during heart-rate measurements. The bodies of animals also slightly and rapidly tremble regardless of respiration or heartbeat, generating moving artifacts. Therefore, Tu et al. proposed a method to reduce respiration harmonics [13]. However, the method is not practical because it uses an extremely long time window to estimate the frequency and power of respiratory harmonics. Subsequently, Tu et al. proposed a practical system that uses multiple FFTs with different window lengths to eliminate respiration harmonics [14]; however, moving artifacts still degraded estimation performance. In addition, Mogi et al. proposed a method based on spectrograms [15]. This method takes advantages of positive and negative frequencies corresponding to cardiac motion and is robust against respiration harmonics, small moving artifacts, and noise.

Petrovi et al. and Son et al. proposed heart rate estimation methods using moving averages and bandpass filter (BPF) for extracting the heartbeat component [16], [17]. Petrovi et al. use a narrow bandpass filter bank (BPFB) [16]. This method switches a bandpass filter to the other bandpass filter of the band containing the heartbeat component and then eliminates respiration harmonics that are out of the band of the selected bandpass filter. In [17], the data recovery procedure doubles the estimated heart rate if the estimated heart rate is excessively low. Yang et al. proposed adaptive noise cancellation and new-type discrete cosine transform (N-DCT) to remove artifacts caused by random body motion [18]. However, this method assumes that the velocity of body motion is constant within a short time window, but in general, the velocity of random body motion is not constant; therefore, this assumption may degrade the estimation performance. Chen et al. proposed the heart-rate measurement based on difference quadratic sum demodulation to prevent the generation of respiration harmonic from [19]. This method requires estimating the heart rate from the components with frequencies corresponding to doubled heart rate, doubled respiration rate, and the sum of respiration and heart rate. However, the unexpected components, other than the three abovementioned three frequencies, occur because of the body movement, and the estimation accuracy is degraded.

In this paper, a heart rate estimation method is proposed that is robust against respiration harmonics, moving artifacts, and noise. The proposed method uses an infinite impulse response-based adaptive notch filter (IIR-ANF) [20], [21] for estimating the respiration frequency in a low frequency band that is occupied by the respiration component. Subsequently, cascaded notch filters, with notch frequencies corresponding to respiration harmonics, prevent interference with heartbeat components. These cascaded notch filters are composed of all-pass filters with substantially narrow notch bands and minimize heartbeat component loss. Finally, the proposed method estimates heart rate using an ANF with an adaptive algorithm from the output signal of cascaded notch filters. An ANF based on all-pass filter with an adaptive algorithm can accurately estimate a notch frequency without the influence of white noise [22]. Animals have large respiration harmonic due to large body movement. and humans have low respiration harmonic due to low body movement. The proposed method improves the accuracy of heart rate estimation in the presence of moving artifacts and noise.

This paper is organized as follows. In Section II, a Doppler radar and the frequency spectrum of a received signal are discussed. The proposed heart rate estimation system, which is robust against respiration harmonics, moving artifacts, and noise, is detailed in Section III. The measurement experiment conduced to evaluate the proposed system is discussed in Section IV. Finally, the paper is concluded in Section V.

II. DOPPLER RADAR

A non-contact heart rate estimation system detects minute periodic vibrations on the body surface caused by heartbeat from a reflected microwave. Assuming that amplitude is ignored, the transmit signal of a Doppler radar is expressed as [1]

$$T(t) = \cos\left[2\pi f_c t + \phi(t)\right], \tag{1}$$

where f_c is the carrier frequency, t is the time index, and $\phi(t)$ is the phase noise of an oscillator. Assuming that the reference distance between a Doppler radar and subject is d_0 and that the displacement due to the motion of the subject's chest is $x(t)$, the distance to the chest from the Doppler radar is expressed as $d(t) = d_0 + x(t)$. When the chest fluctuates before the microwave reaches the subject, the distance between the Doppler radar and chest is $d(t - (d(t)/c))$ at the moment the signal reflects. Therefore, the time delay t_d between transmission and reception can be expressed as [1]

$$t_d = \frac{2d\{t - \frac{d(t)}{c}\}}{c} = \frac{2\{d_0 + x(t - \frac{d(t)}{c})\}}{c}, \tag{2}$$

The respiration-induced chest movement is a 5 cm sinusoid with a 5 second period [1]. However, when d_0 is 1 m, d_0/c is 0.33×10^{-8} seconds. As the motion cycle of the chest is sufficiently larger than d_0/c, the term $d(t)/c$ can be ignored. The received signal of the Doppler radar is delayed by t_d as expressed in (1). When $x(t) \ll d_0$, the received signal $R(t)$ can be approximated as the following equation using (1) and (2) [1].

$$R(t) \approx cos[2\pi f_c t - \frac{4\pi d_0}{\lambda} - \frac{4\pi x(t)}{\lambda} + \phi(t - \frac{2d_0}{c}) + \theta_0], \tag{3}$$

where θ_0 is the phase change on the reflecting surface, and $\lambda = c/f_c$ is the wavelength.

Next, the received signal is multiplied by the transmission signal to only extract the phase shift due to chest movement. The Doppler radar can obtain baseband in-phase/quadrature (I/Q) signals as expressed by the following equations [1].

$$\begin{aligned} I(t) &= \cos\{\theta' + \frac{4\pi x(t)}{\lambda} + \Delta\phi(t)\} + DC_I \\ Q(t) &= \sin\{\theta' + \frac{4\pi x(t)}{\lambda} + \Delta\phi(t)\} + DC_Q, \end{aligned} \tag{4}$$

where $\theta' = 4\pi d_0/\lambda - \theta_0$ and $\Delta\phi(t) = \phi(t) - \phi(t - 2\,d_0/c)$. DC_I and DC_Q are DC offset components in I/Q signals, respectively. Subsequently, the Doppler radar system analyzes the orthogonal I and Q signals.

Then, the effect of respiration components on heart rate estimation is explored using the Fourier series expansion of I/Q signals. The displacement due to chest movement $x(t)$ is expressed as [23]

$$\begin{aligned} x(t) &= x_r(t) + x_h(t) \\ &\approx m_r sin(2\pi f_r t + \psi_{r0}) + m_h sin(2\pi f_h t + \psi_{h0}), \end{aligned} \tag{5}$$

where $x_r(t)$ and $x_h(t)$ represent the physiological movement generated by respiration and heartbeat, respectively. These can be generally modeled as sinusoids with respective: amplitudes as m_r and m_h; frequencies as f_r and f_h; and initial phases as ψ_{r0} and ψ_{h0}. Using (5), I/Q signals are represented by the following equations [23].

$$\begin{aligned} I(t) &= \cos[\frac{4\pi x_r(t)}{\lambda} + \frac{4\pi x_h(t)}{\lambda} + \Phi] + DC_I \\ &= DC_I + \sum_{k=-\infty}^{\infty}\sum_{l=-\infty}^{\infty} J_k(\frac{4\pi m_r}{\lambda}) J_l(\frac{4\pi m_h}{\lambda}) \\ &\quad \cdot \cos(2\pi k f_r t + 2\pi l f_h t + \Phi) \end{aligned} \tag{6}$$

$$\begin{aligned} Q(t) &= \sin[\frac{4\pi x_r(t)}{\lambda} + \frac{4\pi x_h(t)}{\lambda} + \Phi] + DC_Q \\ &= DC_Q + \sum_{k=-\infty}^{\infty}\sum_{l=-\infty}^{\infty} J_k(\frac{4\pi m_r}{\lambda}) J_l(\frac{4\pi m_h}{\lambda}) \\ &\quad \cdot \sin(2\pi k f_r t + 2\pi l f_h t + \Phi), \end{aligned} \tag{7}$$

where the phase term is represented as $\Phi = \theta' + \Delta\phi(t)$ for simplicity. $J_p(\cdot)$ represents the Bessel function of the first kind of p-th order. Equations (6) and (7) indicate that I/Q signals comprise: the fundamental wave of respiration and its harmonics; the fundamental wave of heartbeat and its harmonics; and the intermodulation wave of respiration and heartbeat. Consequently, respiration harmonics degrade heart rate estimation accuracy.

III. PROPOSED HEART RATE ESTIMATION SYSTEM

A. STRUCTURE OF PROPOSED SYSTEM

The proposed heart rate estimation system uses an ANF for eliminating respiration harmonics. Fig. 1 shows the flow of the proposed system, comprising a bandpass filter (BPF), low pass filter (LPF), complex signal demodulation (CSD) component, ANF $H_r(z)$ for estimating respiration frequency, respiration harmonics eliminating filter (RHEF) $H(z)$, and another ANF $H_h(z)$ for estimating heartbeat frequency.

I/Q signals from (4), are converted into discrete-time signals of $I(n)$ and $Q(n)$, where n represents the time index for a discrete-time signal. First, I/Q signals are filtered by the LPF and BPF to separate respiration and heartbeat components. Because respiration frequency is generally smaller than heartbeat frequency, the LPF obtains the fundamental wave of respiration. The BPF separates the components, including heartbeat and respiration harmonics, from the fundamental wave of respiration. The output I/Q signals of the LPF are represented as $I_r(n)$ and $Q_r(n)$, respectively. Similarly, the output I/Q signals of the BPF are represented as $I_h(n)$ and $Q_h(n)$, respectively.

Next, the CSD component is used for combining I/Q signals [23]. The cosine and sine of Φ in (6) and (7) respectively, determine the relative strength between even- and odd-order harmonics. Therefore, the heart rate is difficult to detect because of phase Φ. To solve this problem, the CSD component reconstructs complex signals from I/Q signals. The respective complex input signals for $H_r(z)$ and $H_h(z)$ are

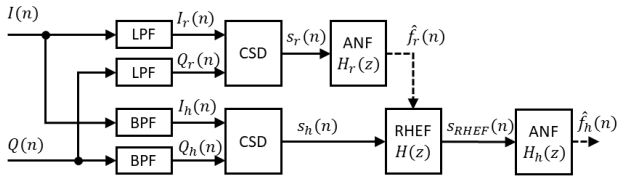

FIGURE 1. Structure of the proposed system.

represented as [23]

$$s_r(n) = I_r(n) + j \cdot Q_r(n) \tag{8}$$

$$s_h(n) = I_h(n) + j \cdot Q_h(n). \tag{9}$$

$H_r(z)$ estimates the respiration frequency as a notch frequency $\hat{f}_r(n)$ of $H_r(z)$ from $s_r(n)$. This filter is explained in detail in Section III-B. Next, $H(z)$, which comprises cascaded notch filters, eliminates respiration harmonics from $s_h(n)$. The output signal of $H(z)$ is represented as $s_{RHEF}(n)$. Section III-C explains the RHEF $H(z)$ in detail. Finally, $H_h(z)$ estimates the heartbeat frequency as a notch frequency $\hat{f}_h(n)$ of $H_h(z)$. The structure of this filter is described in Section III-D. The estimated heart rate $HR_{est}(n)$ (beats per minute (bpm)) is obtained by multiplying $\hat{f}_h(n)$ by 60.

B. RESPIRATION FREQUENCY ESTIMATION

Respiration frequency $f_r(n)$ is estimated using $H_r(z)$. The ANF $H_r(z)$ comprises a 2nd order IIR filter, which has all-pass filter characteristics. The structure of this filter is illustrated in Fig. 2. The transfer function $H_r(z)$ is given by [24]

$$H_r(z) = \frac{1}{2}\frac{(1+\rho_r) + 2\beta_r(n)\, z^{-1} + (1+\rho_r)z^{-2}}{1 + \beta_r(n)\, z^{-1} + \rho_r z^{-2}}, \tag{10}$$

where ρ_r is the squared pole radius of $H_r(z)$, and $\beta_r(n)$ is the tap coefficient related to an estimated respiration frequency $\hat{f}_r(n)$. The output $e_r(n)$ of $H_r(z)$ is represented as

$$e_r(n) = \frac{1}{2}\{s_r(n) + y_r(n)\}, \tag{11}$$

where $y_r(n)$ is an output signal of the 2nd order IIR filter in $H_r(z)$ and expressed as

$$y_r(n) = \rho_r u_r(n) + \beta_r u_r(n-1) + u_r(n-2), \tag{12}$$

where $u_r(n)$ is a tap input signal of the 2nd order IIR filter.

$\beta_r(n)$ controls the notch frequency at which the magnitude response $H_r(z)$ becomes zero as follows [24].

$$\beta_r(n) = -(1+\rho_r)\cos 2\pi\left(\frac{f_r(n)}{F_s}\right), \tag{13}$$

where F_s is the sampling frequency. Since $s_r(n)$ is occupied by the fundamental wave of respiration, the respiration frequency is estimated as the notch frequency. Using (13), the estimated respiration frequency $\hat{f}_r(n)$ is given by

$$\hat{f}_r(n) = \frac{F_s}{2\pi} cos^{-1}\{-\frac{\beta_r(n)}{1+\rho_r}\}, \tag{14}$$

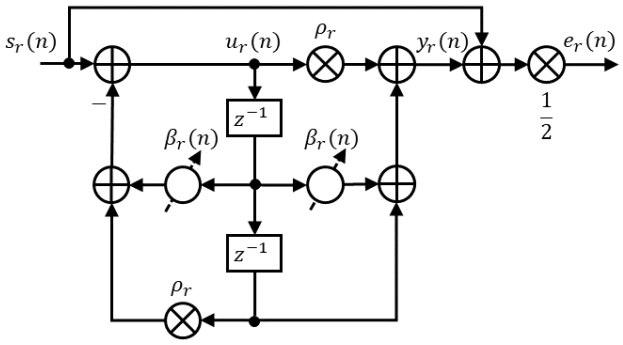

FIGURE 2. Structure of ANF for estimating respiration frequency.

The tap coefficient $\beta_r(n)$ is updated using the following complex normalized least mean square (NLMS) algorithm [25].

$$\beta_r(n+1) = \beta_r(n) - \mu_r \frac{e_r(n)\, u_r^*(n-1)}{u_r^2(n-1)}, \tag{15}$$

where μ_r represents the step size. $*$ denotes the complex conjugate.

C. RESPIRATION HARMONIC ELIMINATION

RHEF $H(z)$ consists of cascaded notch filters. Moreover, notch frequencies are determined by the estimated respiration frequency $\hat{f}_r(n)$, and its transfer function is given by

$$H(z) = \prod_{m=1}^{M} \frac{1}{2}\frac{(1+\rho) + 2\beta_m(n)\, z^{-1} + (1+\rho)z^{-2}}{1 + \beta_m(n)\, z^{-1} + \rho z^{-2}}, \tag{16}$$

where M represents the number of stages of a notch filter, ρ represents the squared pole radius, and β_m represents the tap coefficient corresponding to the $(m+1)$-th harmonic frequency of respiration. $\beta_m(n)$ is expressed as [24]

$$\beta_m(n) = -(1+\rho)\cos\{2\pi\frac{(m+1)\hat{f}_r(n)}{F_s}\}, \tag{17}$$

The notch frequencies of $H(z)$ change according to the estimated respiration frequency $\hat{f}_r(n)$. Thus, the proposed system can obtain a signal that attenuates the respiration harmonics interfering with heartbeat components as the output signal of $H(z)$. The notch band of notch filters is substantially narrow, and the RHEF minimizes the loss of heartbeat components.

D. HEARTBEAT FREQUENCY ESTIMATION

The transfer function $H_h(z)$ is expressed as [24]

$$H_h(z) = \frac{1}{2}\frac{(1+\rho_h) + 2\beta_h(n)\, z^{-1} + (1+\rho_h)z^{-2}}{1 + \beta_h(n)\, z^{-1} + \rho_h z^{-2}}, \tag{18}$$

where ρ_h is the squared pole radius of $H_h(z)$, and $\beta_h(n)$ is the tap coefficient related to heart rate. The output of this filter $e_h(n)$ is represented as

$$e_h(n) = \frac{1}{2}\{s_{RHEF}(n) + y_h(n)\}, \tag{19}$$

where $y_h(n)$ is an output signal of the 2nd order IIR filter in $H_h(z)$ and expressed by

$$y_h(n) = \rho_h u_h(n) + \beta_h u_h(n-1) + u_h(n-2), \quad (20)$$

where $u_h(n)$ is a tap input signal of the 2nd order IIR filter in $H_h(z)$,

The estimated heartbeat frequency $\hat{f}_h(n)$ is defined from the notch frequency and tap coefficient $\beta_h(n)$, as follows:

$$\hat{f}_h(n) = \frac{F_s}{2\pi} cos^{-1}\{-\frac{\beta_h(n)}{1+\rho_h}\}, \quad (21)$$

using the relationship between a notch frequency of an ANF and tap coefficient [24]. The tap coefficient $\beta_h(n)$ is updated using the following complex NLMS algorithm [25].

$$\beta_h(n+1) = \beta_h(n) - \mu_h \frac{e_h(n)\, u_h^*(n-1)}{u_h^2(n-1)}, \quad (22)$$

where μ_h represents the step size for $H_h(z)$.

Let us consider the influence of moving artifacts and noise on an ANF with NLMS algorithm. The numerator of updating term $e_h(n)\, u_h^*(n-1)$ represents instantaneous estimates of $E[e_h(n)\, u_h^*(n-1)]$ in a steepest-descent algorithm. Moreover, the least mean square algorithm, which is recursive, effectively estimates $E[e_h(n)\, u_h^*(n-1)]$ using time averaging [25]. When the input signal of the ANF is white, $E[e_h(n)\, u_h^*(n-1)]$ is zero because of the orthogonality associated with an all-pass filter [22]. Thus, assuming that noise and moving artifacts are white in nature, they do not influence heart rate estimation. Even if noise and moving artifacts are colored (no-white) in nature, an ANF with NLMS algorithm is expected to eliminate their influence in the case that their frequency characteristics are close to white. Moreover, in case that an animal suddenly moves, e.g., sitting and then standing posture, moving artifacts occur suddenly and their probability characteristics drastically change in a short time duration. As the adaptive algorithm neglects the moving artifact components in $E[e_h(n)\, u_h^*(n-1)]$ due to the time-variance of a moving artifact, an ANF with NLMS algorithm is robust against moving artifacts.

IV. MEASUREMENT EXPERIMENT

A. DOPPLER RADAR SETUP AND EVALUATION

A computer simulation is conducted to evaluate the performance of the proposed system. The Doppler radar module used in this experiment is SHARP DC6M4JN3000 with one transmitter antenna and one receiver antenna. Its carrier frequency is 24 GHz with a maximum output power of 10 dBm. The H plane and E plane beam widths are 25° and 20°, respectively. The gain of the horn antennas is 20 dBi. The module comprises the LPF and BPF. It outputs discrete-time I/Q signals ($I_r(n)$, $Q_r(n)$, $I_h(n)$, and $Q_h(n)$) with a 50-Hz sampling frequency.

To evaluate the estimated heart rate, we used the mean absolute percentage error (MAPE), mean absolute error (MAE), mean squared error (MSE), and root mean squared error (RMSE) which were defined as

TABLE 1. Simulation parameters for human subjects.

Pole radius ρ_h for $H_h(z)$	0.95
Step size μ_h for $H_h(z)$	0.1
Initial value of estimated heart rate for $\beta_h(0)$	120 [bpm]
Pole radius ρ_r for $H_r(z)$	0.99
Initial value of estimated respiration rate for $\beta_r(0)$	20 [bpm]
Step size μ_r for $H_r(z)$	0.05

$$MAPE = \frac{1}{K}\sum_{i=1}^{K} \frac{|HR_{ref}(i) - HR_{est}(i)|}{HR_{ref}(i)} \times 100[\%], \quad (23)$$

$$MAE = \frac{1}{K}\sum_{i=1}^{K} |HR_{ref}(i) - HR_{est}(i)|, \quad (24)$$

$$MSE = \frac{1}{K}\sum_{i=1}^{K} \{HR_{ref}(i) - HR_{est}(i)\}^2, \quad (25)$$

$$RMSE = \sqrt{\frac{1}{K}\sum_{i=1}^{K} \{HR_{ref}(i) - HR_{est}(i)\}^2}, \quad (26)$$

where $|\cdot|$ represents the absolute value, K is the number of samples, $HR_{est}(i)$ is the estimated heart rate at the i-th sample, and $HR_{ref}(i)$ is the heart rate measured by a contact-type device.

B. MEASUREMENT EXPERIMENTS FOR HUMAN SUBJECTS

1) MEASUREMENT CONDITIONS FOR HUMAN SUBJECTS

This section provides details of the experiments conducted on humans who can remain stationary to evaluate only the reduction performance of the respiration harmonics of the proposed method. Table 1 lists the parameters of the proposed system used in this experiment. The NLMS algorithm converges if and only if $0 < \mu < 2$ [25]. When μ is 1, the convergence speed of NLMS algorithm is fastest [26]. If tap input signals include disturbance and optimal tap coefficients are nonstationary, optimum step size is given by signal to noise ratio (SNR) of tap input signal and power of optimal tap coefficient fluctuation [27]. As SNR and power of optimal tap coefficient fluctuations are unknown, the step size is generally set to $0 < \mu < 1$. The pole radius with $0 < \sqrt{\rho} < 1$ is set to slightly less than 1. The notch band, the area removed by the adaptive notch filter narrows as the radius approaches 1 [21].

The distance between a subject's chest and the Doppler radar was set as 1 m, and the subjects are kept in a seated posture. The subjects wore a T-shirt during the experiment. The true heartbeat and respiration rates were measured by a contact-type vital sensor (Equivital Ltd., EQ02) simultaneously with the measurements by the Doppler radar. Each recording is measured for 200 second. As the contact-type sensor detects heart rate every 5 second, the estimated values are also obtained every 5 second for comparison.

TABLE 2. Average and deviation of true heart rate for human subjects.

Subject No.	Average	Maximum Deviation	Standard Deviation
1	86.15	3.85	1.98
2	72.17	10.83	2.75
3	77.24	12.76	4.06
4	82.12	6.88	3.19
5	69.32	11.68	5.12
6	85.22	6.78	3.64
7	64.78	38.22	7.71
8	74.88	15.12	4.03

A dataset is created for each person for the experiments, comprising eight people as subjects with ages ranging from 21 to 25 years. This experiment on human subjects was approved by the research ethics review committee of the Faculty of Engineering, Tottori university (No. R4-5). Table 2 shows each human subject's average value, maximum deviation, and standard deviation of heart rate data, which is detected by the contact-type vital sensor. The maximum deviation is given by

$$Maximum\ deviation = \max\{|HR_{ref}(i) - \overline{HR_{ref}(i)}|\}, \quad (27)$$

where $\overline{HR_{ref}(i)}$ represents the time-average of $HR_{ref}(i)$. $\max\{\cdot\}$ represents maximum value of $\{\cdot\}$.

2) NUMBER OF STAGES AND POLE RADIUS OF RHEF FOR HUMAN SUBJECTS

The RHEF $H(z)$ used in the proposed system comprises notch filters connected in cascade. The number of removed respiration harmonics depends on the number of notch-filter stages. Moreover, the pole radius determines the notch bandwidth. Therefore, the accuracy of heart rate estimation depends on the number of stages and the pole radius of the RHEF $H(z)$.

Fig. 3 illustrates the MAPE of heart rate versus the number of stages of RHEF $H(z)$. The MAPE in Fig. 3 are obtained by averaging the results of eight subjects. The number of stages in filter cascade $M = 0$ represents the proposed system without the RHEF. The simulation results show that the error for $M = 2$ is smaller than that for $M = 0$, and the introduction of the RHEF improves the accuracy of heart rate estimation. Unfortunately, the error increases when the number of stages is greater than or equal to three and when the pole radius reduces. This is because the number of stages is too many and the notch bandwidth is too wide to reduce respiration harmonics; thus, the RHEF distorts a heartbeat component. When $\rho = 0.95$ at the second stage of the cascaded notch filters, the proposed system sufficiently reduces the error. Therefore, $\rho = 0.95$ and $M = 2$ are adopted for the filter cascade.

3) EXPERIMENT RESULTS FOR HUMAN SUBJECTS

Table 3 illustrates the simulation results in heart rate estimation to compare the proposed method with the conventional methods. Each value of the evaluation indexes is obtained from eight subjects, and the average value represents averaging the results of eight subjects. The proposed method's average MAPE, MAE, MSE, and RMSE are 5.24%, 4.00, 28.38, and 5.26, respectively, and the proposed method obtains the highest accuracy. In addition, all evaluation indexes of the proposed method are lower than any other conventional methods in each trial.

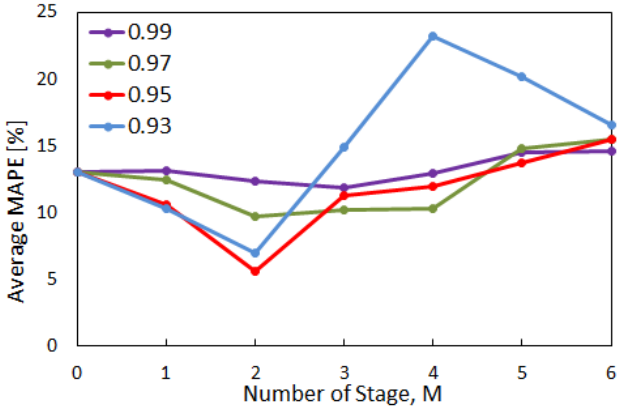

FIGURE 3. Average MAPE vs. the number of stages of the RHEF for human subjects.

Figs. 4 shows the estimated heart rate for the human subject No. 1. Figs. 4(a), (b), (c), (d), (e), (f), and (g) illustrate the heart rate estimated using the aforementioned conventional methods. Fig. 4(h) illustrates the heart rate estimated using the proposed system. Fig. 5 shows the power spectrums of the input and output signals of the RHEF $H(z)$. Fig. 5 (a), and (b) illustrate the power spectrum at 100 and 180 second, respectively. Considering Fig. 5, the input signal of the RHEF includes 3rd order respiration harmonic. The frequencies of the 3rd order harmonics are respectively 1.074 Hz (64.44 bpm) at 100 second and 1.07 Hz (64.2 bpm) at 180 second. Moreover, the contact-type vital sensor indicates heart rates of 1.51 Hz (90.6 bpm) at 100 second and 1.46 Hz (87.6 bpm) at 180 second.

Figs. 4(a), (b), and (c) show that autocorrelation, FFT, and CWT sometimes can be detected the heart rate accurately; however, they are not always usable. Fig. 5 (b) shows that they are not influenced by 3rd order respiration harmonic, whose power is lower than the heartbeat component. Moreover, the 3rd order respiration harmonic, whose power is higher than the heartbeat component, degrades the estimation accuracy from Fig. 5 (a).

Fig. 4(d) shows that the time-window-variation method detects the heart rate with slight error. Fig. 4(e) shows that the spectrogram method degrades estimation performance owing to respiration harmonics and noise. Fig. 4(f) shows that the heart rate estimated by BPFB is off the reference because BPFB traces the 3rd order respiration harmonic in the band of a selected bandpass filter. As indicated by Fig. 4(g), N-DCT cannot reliably capture the true heart rate due to 3rd order respiration harmonic and noise. Fig. 4(h) shows that the proposed method can trace the reference. Fig. 5 shows that the RHEF $H(z)$ with cascaded notch filters reduces the 3rd

TABLE 3. Simulation results for human subjects.

Evaluation Index	Subject No.	Auto-correlation	FFT	CWT	TWV	Spectrogram	BPFB	N-DCT	Proposed Method
MAPE	1	17.13	16.01	18.71	6.56	25.10	39.48	20.30	2.67
	2	8.20	10.40	9.69	24.53	39.58	30.37	23.70	6.32
	3	11.61	18.12	14.67	15.86	27.56	37.32	18.05	5.28
	4	15.30	20.92	17.40	11.69	32.03	38.31	21.14	6.10
	5	8.13	13.18	9.91	29.65	42.62	17.38	23.74	5.36
	6	21.02	26.93	24.71	5.38	22.81	36.80	24.66	4.26
	7	8.25	8.47	8.48	35.70	39.83	21.49	28.72	7.65
	8	12.58	14.07	14.39	19.93	29.00	29.95	19.24	4.29
	Average	12.78	16.01	14.75	18.66	32.32	31.39	22.44	5.24
MAE	1	14.81	13.92	16.14	5.64	21.67	34.12	17.53	2.28
	2	5.94	7.51	7.01	17.62	28.57	21.89	17.04	4.52
	3	9.06	13.99	11.44	12.06	21.39	28.69	13.80	4.21
	4	12.73	17.41	14.53	9.51	26.41	31.72	17.40	5.09
	5	5.67	9.38	6.90	20.02	29.32	12.29	16.26	3.63
	6	18.04	23.11	21.09	4.55	19.59	31.54	21.12	3.70
	7	5.72	5.80	5.81	22.55	25.55	14.64	18.69	5.29
	8	9.41	10.55	10.76	14.74	21.43	22.26	14.28	3.28
	Average	10.17	12.71	11.71	13.34	24.24	24.64	17.01	4.00
MSE	1	366.14	377.14	412.55	39.79	737.44	1187.30	472.05	14.71
	2	54.27	89.78	73.22	335.23	1552.80	493.24	369.41	34.23
	3	129.41	234.45	181.76	160.25	750.95	834.92	247.97	36.10
	4	221.58	387.35	292.11	115.03	1279.60	1024.70	415.72	37.22
	5	50.62	128.96	64.10	441.55	1400.50	175.57	356.50	18.55
	6	410.01	622.51	520.24	30.69	611.34	1026.10	592.51	26.70
	7	71.10	67.47	62.75	542.85	1156.30	292.92	541.29	37.06
	8	114.82	149.18	148.73	229.65	891.33	539.98	275.95	22.52
	Average	177.24	257.11	219.43	236.88	1047.53	696.84	408.93	28.38
RMSE	1	19.13	19.42	20.31	6.31	27.16	34.46	21.73	3.84
	2	7.37	9.48	8.56	18.31	39.41	22.21	19.22	5.85
	3	11.38	15.31	13.48	12.66	27.40	28.90	15.75	6.01
	4	14.89	19.68	17.09	10.73	35.77	32.01	20.39	6.10
	5	7.12	11.36	8.01	21.01	37.42	13.25	18.88	4.31
	6	20.25	24.95	22.81	5.54	24.73	32.03	24.34	5.17
	7	8.43	8.21	7.92	23.30	34.00	17.12	23.27	6.09
	8	10.72	12.21	12.20	15.15	29.86	23.24	16.61	4.75
	Average	12.41	15.08	13.80	14.13	31.97	25.40	20.02	5.26

order respiration harmonic, allowing the proposed system to estimate heart rate accurately. In addition, Fig. 4(h) shows that the proposed method using the ANF with adaptive algorithm is more robust against noise than the time-window-variation method.

C. MEASUREMENT EXPERIMENTS FOR DOG SUBJECT

1) MEASUREMENT CONDITIONS FOR DOG SUBJECT

The performance of the proposed system is evaluated for a beagle dog as a subject. The aim of dog experiments is to evaluate the estimation accuracy of the proposed method under the influence of respiration harmonics and body movement. The dog moves, sits, or lies down in a cage as well as slightly and rapidly trembles. Table 4 lists the parameters of the proposed system used in this experiment.

A dataset is created that contains seven recordings on a 13-year-old female dog at Veterinary Medical Center, Tottori University. This experiment on the dog was approved by Institutional Animal Care and USE Committee, Tottori University (Approval No. 19-T-4). The dog's condition in the experiment differs from that in a daily life environment, and the dog's mood changes from day to day. The Doppler radar is attached vertically downward at the center position of the ceiling of a wire pet cage as shown in Fig. 6. The dog is constantly below the radar; however, the distance between the radar and the body surface changes depending on dog's body posture. When the dog sits, the distance is approximately 5 cm above the head, whereas when dog lies down, it becomes 30 cm above abdomen. Each recording is measured for 40 min. Simultaneously, the ground truth heart rate is recorded using an electrocardiography-type (ECG) vital sign monitor (Nihon koden Corp. BSM-3592). Table 5 shows each trial's average, maximum, and standard deviation of heart rate data, which are detected by the contact-type vital sensor.

MAPE, MAE, MSE, and RMSE were used for evaluating the estimated heart rate. As the vital sensor detects heart rate every 1 second, an estimated heart rate is set to output every 1 second for comparison. Because a received signal for a dog includes many artifacts due to the misalignment of electrodes, $HR_{ref}(i)$ is obtained using a moving average for 30 second to reduce artifacts.

2) NUMBER OF STAGES AND POLE RADIUS OF THE RHEF FOR DOG SUBJECT

The effects of respiratory harmonics are different because of the difference in body structures between humans and

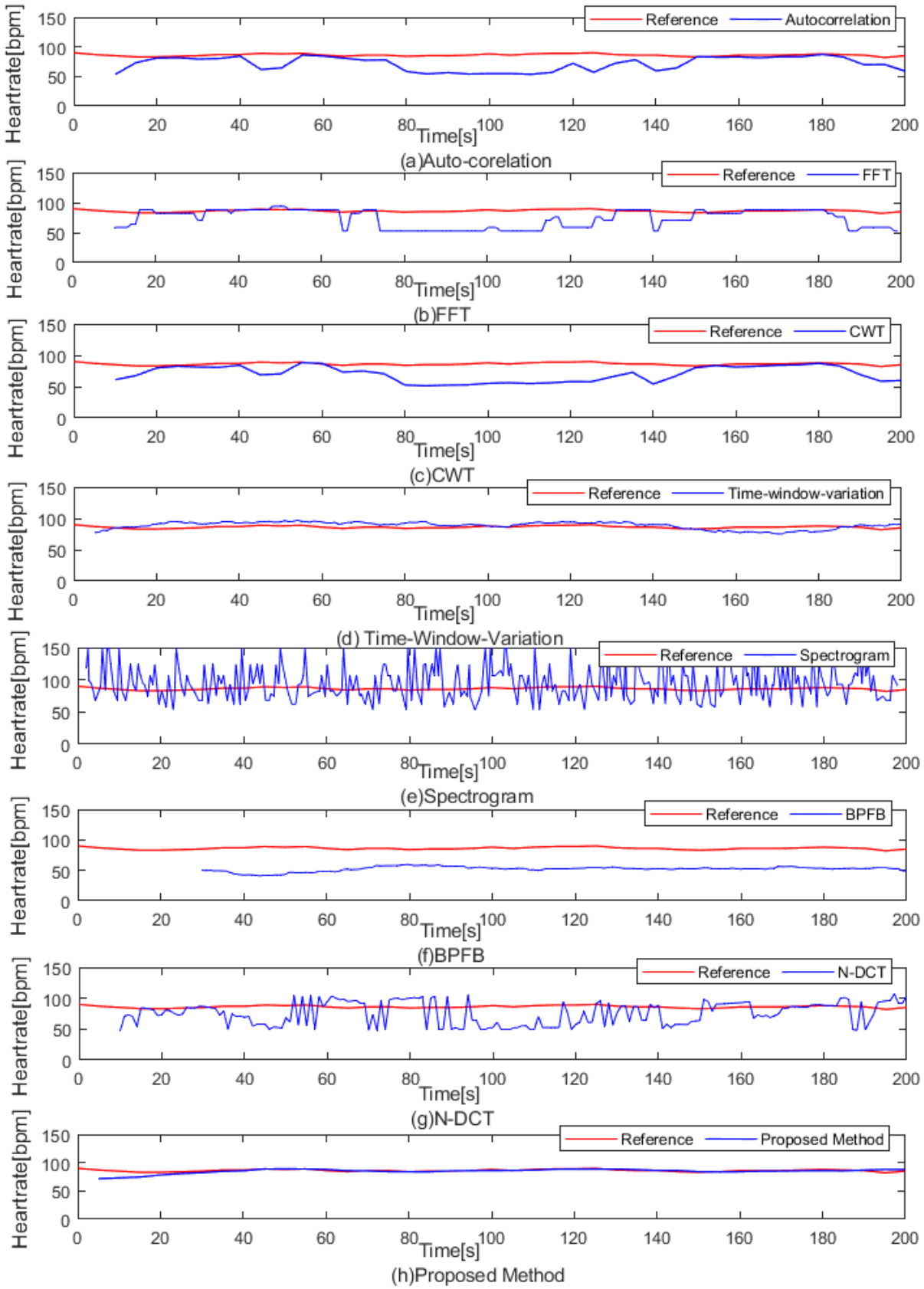

FIGURE 4. Estimated heart rate for human subject No. 1.

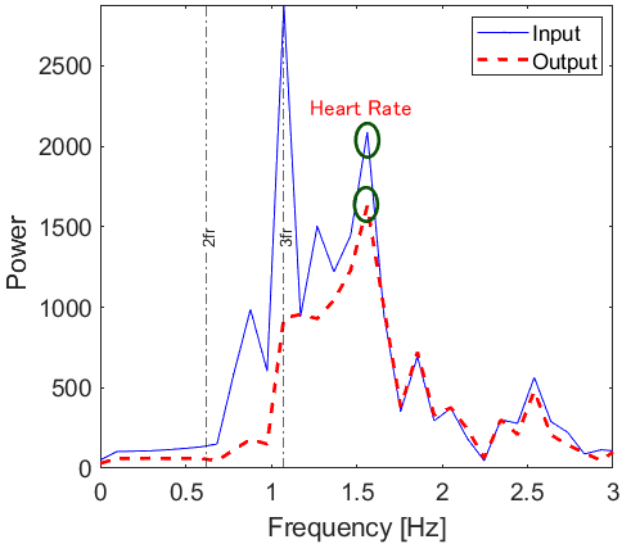

(a) 100 second

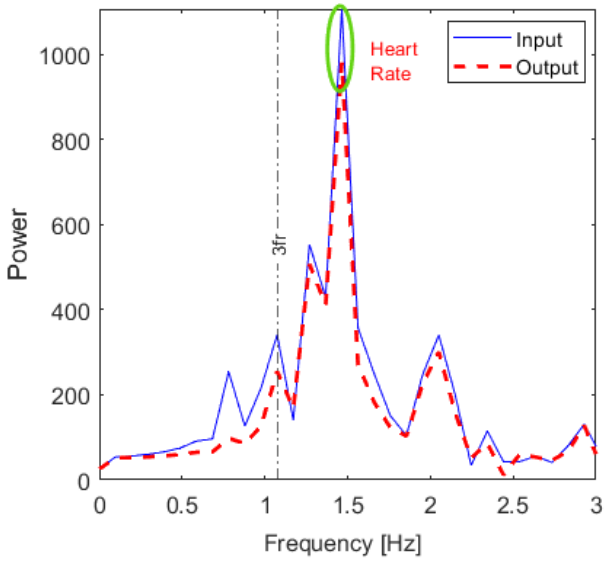

(b) 180 second

FIGURE 5. Input and output power spectrums of the RHEF for human subject No.1.

TABLE 4. Simulation parameters for the dog subject.

Pole radius ρ_h for $H_h(z)$	0.95
Step size μ_h for $H_h(z)$	0.1
Initial value of estimated heart rate for $\beta_h(0)$	120 [bpm]
Pole radius ρ_r for $H_r(z)$	0.99
Initial value of estimated respiration rate for $\beta_r(0)$	20 [bpm]
Step size μ_r for $H_r(z)$	0.05

dogs, and the required number of RHEF stages also differ. Therefore, we conduct the experiments on the number of RHEF stages for a dog. Fig. 7 illustrates the MAPE of heart rate versus the number of stages of the RHEF $H(z)$. The MAPE in Fig. 7 are obtained by averaging the results of seven trials. The stage of zero represents the proposed system

FIGURE 6. Scene of data collection for the dog subject.

TABLE 5. Average and deviation of true heart rate for the dog subject.

Trial No.	Average	Maximum Deviation	Standard Deviation
1	136.93	61.07	14.36
2	161.43	56.57	13.50
3	140.58	58.42	15.60
4	152.07	58.93	16.16
5	135.65	67.35	18.83
6	156.50	63.50	14.24
7	148.96	48.04	13.91

without the RHEF $H(z)$. The simulation results indicates that the RHEF $H(z)$ effectively improves estimation accuracy. Unfortunately, the error increases when the number of stages is greater than or equal to five for $\rho = 0.93$, 0.95, and 0.97. This is because the notch bandwidth is too wide to reduce respiration harmonics; thus, the RHEF distorts heartbeat components.

When $\rho = 0.99$, the proposed system slightly reduces the error because the notch bandwidth is too narrow. Notably, respiration harmonics may remain when the estimated respiration frequency is slightly different from the true respiration frequency. When $\rho = 0.95$ with $M = 4$, the proposed system sufficiently reduces error. Therefore, $\rho = 0.95$ and $M = 4$ are adopted for the RHEF.

3) HEART RATE ESTIMATION PERFORMANCE FOR DOG

The proposed system is compared with conventional systems based on autocorrelation [1], FFT [1], CWT [12], TWV [14], spectrogram method [15], BPFB [16], and N-DCT [18]. The MAPE, MAE, MSE, and RMSE are shown in Table 6. The proposed method's MAPE, MAE, MSE, and RMSE are7.04%, 10.28, 165.31, and 12.58 on average, respectively, and the proposed method obtains higher accuracy than any other methods. The proposed method improves the estimation accuracy for all evaluation indexes in each trial.

Fig. 8 illustrates the estimated heart rate of trial #7. Fig. 8(a) shows the heart rate obtained from an ECG signal before and after moving average. Figs. 8(b), (c), (d), (e), (f), (g), and (h) show the heart rate estimated using autocorrelation, FFT, CWT, time-window-variation technique,

TABLE 6. Simulation results for the dog subject.

Evaluation Index	Trial No.	Auto-correlation	FFT	CWT	TWV	Spectrogram	BPFB	N-DCT	Proposed Method
MAPE	1	27.08	19.14	39.26	21.54	28.66	43.82	50.27	11.42
	2	16.21	30.77	50.27	15.37	36.45	53.04	48.19	6.10
	3	23.16	18.83	35.63	20.85	29.91	45.14	48.76	6.00
	4	21.16	26.35	45.87	17.66	32.93	49.47	48.20	6.08
	5	26.78	19.89	36.87	23.16	29.91	44.38	49.89	8.43
	6	18.93	28.81	47.46	16.75	35.05	50.96	48.08	5.92
	7	21.74	26.09	44.82	18.53	31.91	48.25	49.17	5.34
	Average	22.15	24.27	42.88	19.13	32.12	47.86	48.94	7.04
MAE	1	36.46	26.53	54.14	29.25	39.67	60.41	68.84	15.17
	2	26.06	49.61	81.37	24.79	59.31	85.96	77.70	10.03
	3	32.34	26.82	50.41	28.98	42.38	63.70	68.57	8.44
	4	31.48	40.22	69.99	26.43	50.99	75.77	73.19	9.36
	5	35.56	27.41	50.34	30.81	41.02	60.81	67.54	11.58
	6	29.45	45.17	74.28	26.02	55.33	80.11	75.27	9.48
	7	31.85	39.07	67.16	27.19	48.13	72.35	73.14	7.89
	Average	31.89	36.40	63.96	27.64	48.12	71.30	72.04	10.28
MSE	1	1523.7	1015.2	3164.9	1224.5	2153.9	3781.1	4991.9	331.06
	2	1066.2	3118.6	6790.2	1303.9	4411.3	7511.5	6795.2	147.96
	3	1256.4	1062.3	2910.2	1173.7	2427.3	4157.9	5039.3	106.56
	4	1276.8	2058.8	5159.3	1248.3	3480.9	5931.8	5909.6	131.47
	5	1536.9	1060.5	2785.2	1237.5	2291.4	3871.7	4878.3	200.47
	6	1151.7	2527.8	5714.0	1276.5	3902.3	6529.2	6279.0	143.41
	7	1269.1	1960.6	4769.4	1222.2	3099.9	5393.2	5776.5	96.11
	Average	1297.2	1829.1	4470.4	1240.9	3109.5	5310.9	5667.1	165.31
RMSE	1	39.04	31.86	56.26	34.99	46.41	61.49	70.65	18.20
	2	32.65	55.84	82.40	36.11	66.42	86.67	82.43	12.16
	3	35.45	32.59	53.95	34.26	49.27	64.48	70.99	10.32
	4	35.73	45.37	71.83	35.33	59.00	77.02	76.87	11.47
	5	39.20	32.56	52.78	35.18	47.87	62.22	69.84	14.16
	6	33.94	50.28	75.59	35.73	62.47	80.80	79.24	11.98
	7	35.62	44.28	69.06	34.96	55.68	73.44	76.00	9.80
	Average	35.95	41.83	65.98	35.22	55.30	72.30	75.15	12.58

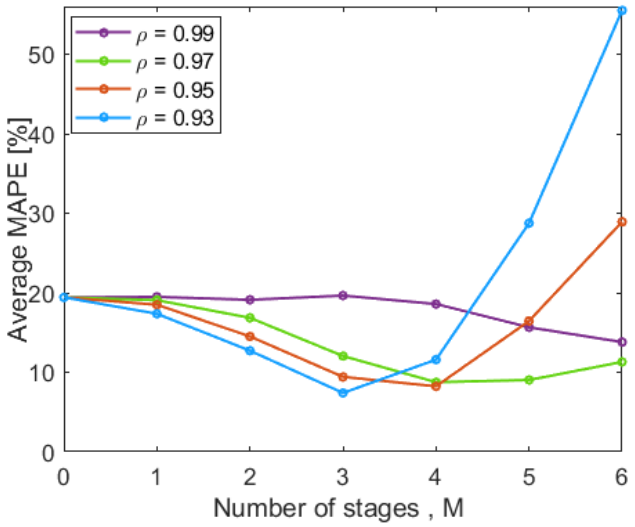

FIGURE 7. Average MAPE vs. the number of stages of the RHEF for the dog subject.

spectrogram, BPFB, and N-DCT, respectively. Fig. 8(i) illustrates the heart rate estimated using the proposed system. Fig. 9 shows the power spectrum of the input and output signals of the RHEF $H(z)$ at 2,230 seconds into trial #7. The RHEF input signal contains components at 1.48 Hz, 1.85 Hz, and 2.3 Hz. AS the respiration frequency estimated by the proposed method is 0.37 Hz at 2,230 seconds, the 1.48 Hz and 1.85 Hz components are the fourth and fifth respiratory harmonics. Because the true heart rate measured using the ECG vital sign monitor is 138 bpm (2.3 Hz) at 2,230 seconds, the 2.3 Hz component in Fig. 9 is the heart-rate component.

Figs. 8(b), (c), (e), (f), and (h) show that the heart rates estimated with autocorrelation, FFT, time-window-variation, spectrogram, and N-DCT significantly vary because of moving artifacts. Although the heart rates estimated with CWT and BPFB are low dispersion as shown in Figs. 8(d), and (g), respectively, these methods capture 4th and 5th respiration harmonics. Fig. 8(i) shows that the proposed method tracks true heart rate accurately. As the RHEF $H(z)$ with $M = 4$ reduces the 4th and 5th respiration harmonics as shown in Fig. 9, the proposed method improves the estimation accuracy by eliminating respiration harmonics. Moreover, the proposed method is robust against moving artifacts and noise because the heart rates estimated with the proposed method are low dispersion as demonstrated in Fig. 8(i). Simulation results show that the proposed method, which uses ANF and adaptive algorithm, demonstrably improves the accuracy of heart rate estimation.

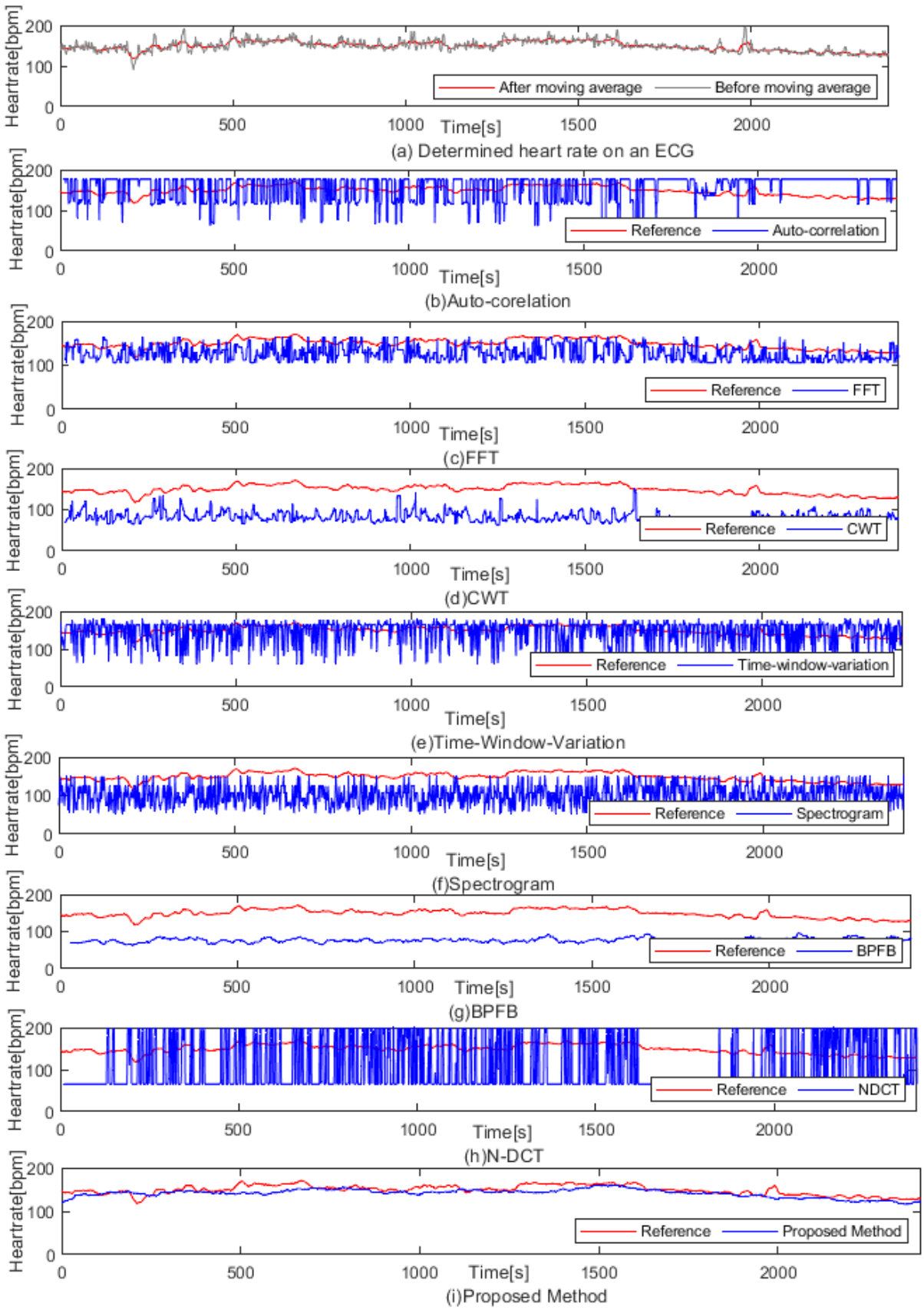

FIGURE 8. Estimated heart rate for the dog subject (Trial No. 7).

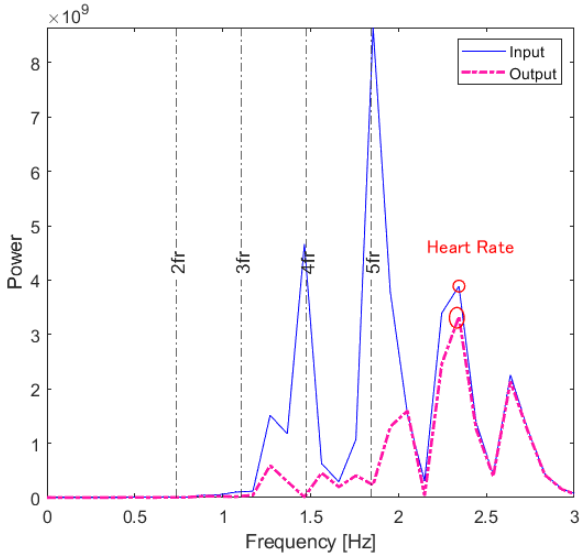

FIGURE 9. Input and output power spectrums of the RHEF for the dog subject (Trial No. 7) at 2,230 s.

V. CONCLUSION

In this paper, a novel heart rate estimation method is proposed using an ANF and RHEF. Conventional heart rate estimation systems degrade estimation accuracy because of respiration harmonics, moving artifacts, and noise. To this end, the proposed system eliminates respiration harmonics using cascaded notch filters with notch frequencies that are controlled by an estimated fundamental respiration frequency. In addition, an ANF with an adaptive algorithm is adopted to attain robust estimation against moving artifacts and noise. Considering the experimental results for human and dog subjects, the proposed method achieves the best performance in comparison with multiple conventional methods. This indicates that the proposed method demonstrably estimates heart rate accurately without the influence of respiration harmonics, moving artifacts, and noise.

In the future, we will investigate automatically setting hyper parameters and improvement of estimation accuracy for a received signal with intermodulation of respiration and heart rate.

REFERENCES

[1] A. D. Droitcour, "Non-contact measurement of heart and respiration rates with single chip microwave Doppler radar," Ph.D. dissertation, Dept. Elect. Eng., Stanford Univ., Stanford, CA, USA, 2006.

[2] P.-H. Juan, F.-K. Wang, and Y.-T. Tzeng, "SIL-radar-based rat detector for warehouse management system," in *IEEE MTT-S Int. Microw. Symp. Dig.*, May 2019, pp. 1–4, doi: 10.1109/IMBIOC.2019.8777772.

[3] M. Garbey, N. Sun, A. Merla, and I. Pavlidis, "Contact-free measurement of cardiac pulse based on the analysis of thermal imagery," *IEEE Trans. Biomed. Eng.*, vol. 54, no. 8, pp. 1418–1426, Aug. 2007, doi: 10.1109/TBME.2007.891930.

[4] A. Parnandi and R. Gutierrez-Osuna, "Contactless measurement of heart rate variability from pupillary fluctuations," in *Proc. Humaine Assoc. Conf. Affect. Comput. Intell. Interact.*, Sep. 2013, pp. 191–196, doi: 10.1109/ACII.2013.38.

[5] W. Verkruysse, L. O. Svaasand, and J. S. Nelson, "Remote plethysmographic imaging using ambient light," *Opt. Exp.*, vol. 16, no. 26, pp. 21434–21445, 2008.

[6] K. Alghoul, S. Alharthi, A. El Saddik, and H. Al Osman, "Heart rate variability extraction from videos signals: ICA vs. EVM comparison," *IEEE Access*, vol. 5, pp. 4711–4719, 2017, doi: 10.1109/ACCESS.2017.2678521.

[7] S. Sanyal and K. K. Nundy, "Algorithms for monitoring heart rate and respiratory rate from the video of a user's face," *IEEE J. Transl. Eng. Health Med.*, vol. 6, pp. 1–11, 2018, doi: 10.1109/JTEHM.2018.2818687.

[8] N. Sharma, S. Kaman, and P. K. Mahapatra, "Non-contact measurement of human heart rate using low cost video camera," in *Proc. 5th Int. Conf. Image Inf. Process. (ICIIP)*, Nov. 2019, pp. 58–62, doi: 10.1109/ICIIP47207.2019.8985746.

[9] D. Cho and B. Lee, "Non-contact robust heart rate estimation using HSV color model and matrix-based IIR filter in the face video imaging," in *Proc. 38th Annu. Int. Conf. IEEE Eng. Med. Biol. Soc. (EMBC)*, Aug. 2016, pp. 3847–3850, doi: 10.1109/EMBC.2016.7591567.

[10] S. Ding, Z. Ke, Z. Yue, C. Song, and L. Lu, "Noncontact multi-physiological signals estimation via visible and infrared facial features fusion," *IEEE Trans. Instrum. Meas.*, vol. 71, pp. 1–13, 2022, doi: 10.1109/TIM.2022.3209750.

[11] C. Li, J. Ling, J. Li, and J. Lin, "Accurate Doppler radar noncontact vital sign detection using the RELAX algorithm," *IEEE Trans. Instrum. Meas.*, vol. 59, no. 3, pp. 687–695, Mar. 2010, doi: 10.1109/TIM.2009.2025986.

[12] A. Tariq and H. Ghafouri-Shiraz, "Vital signs detection using Doppler radar and continuous wavelet Transform," in *Proc. 5th Eur. Conf. Antennas Propag. (EUCAP)*, 2011, pp. 285–288.

[13] J. Tu and J. Lin, "Respiration harmonics cancellation for accurate heart rate measurement in non-contact vital sign detection," in *IEEE MTT-S Int. Microw. Symp. Dig.*, Jun. 2013, pp. 1–3, doi: 10.1109/MWSYM.2013.6697732.

[14] J. Tu and J. Lin, "Fast acquisition of heart rate in noncontact vital sign radar measurement using time-window-variation technique," *IEEE Trans. Instrum. Meas.*, vol. 65, no. 1, pp. 112–122, Jan. 2016, doi: 10.1109/TIM.2015.2479103.

[15] E. Mogi and T. Ohtsuki, "Heartbeat detection with Doppler radar based on spectrogram," in *Proc. IEEE Int. Conf. Commun. (ICC)*, May 2017, pp. 1–6, doi: 10.1109/ICC.2017.7996378.

[16] V. L. Petrovic, M. M. Jankovic, A. V. Lupsic, V. R. Mihajlovic, and J. S. Popovic-Bozovic, "High-accuracy real-time monitoring of heart rate variability using 24 GHz continuous-wave Doppler radar," *IEEE Access*, vol. 7, pp. 74721–74733, 2019, doi: 10.1109/ACCESS.2019.2921240.

[17] N. H. Son, H. T. Yen, G. Sun, and K. Ishibashi, "High-accuracy heart rate estimation by half/double BBI moving average and data recovery algorithm of 24 GHz CW-Doppler radar," in *Proc. Int. Conf. Adv. Technol. Commun. (ATC)*, Oct. 2022, pp. 360–363, doi: 10.1109/ATC55345.2022.9943010.

[18] Z.-K. Yang, H. Shi, S. Zhao, and X.-D. Huang, "Vital sign detection during large-scale and fast body movements based on an adaptive noise cancellation algorithm using a single Doppler radar sensor," *Sensors*, vol. 20, no. 15, p. 4183, Jul. 2020, doi: 10.3390/s20154183.

[19] X. Chen and X. Ni, "Noncontact sleeping heartrate monitoring method using continuous-wave Doppler radar based on the difference quadratic sum demodulation and search algorithm," *Sensors*, vol. 22, no. 19, p. 7646, Oct. 2022, doi: 10.3390/s22197646.

[20] P. A. Regalia, S. K. Mitra, and P. P. Vaidyanathan, "The digital all-pass filter: A versatile signal processing building block," *Proc. IEEE*, vol. 76, no. 1, pp. 19–37, Jan. 1988, doi: 10.1109/5.3286.

[21] P. A. Regalia, *Adaptive IIR Filtering in Signal Processing and Control*. New York, NY, USA: Marcel Dekker, 1995.

[22] J. Okello, S. Arita, Y. Itoh, Y. Fukui, and M. Kobayashi, "An adaptive notch filter for eliminating multiple sinusoids with reduced bias," in *Proc. IEEE Int. Symp. Circuits Syst.*, May 2000, pp. 551–554, doi: 10.1109/ISCAS.2000.856119.

[23] C. Li and J. Lin, "Complex signal demodulation and random body movement cancellation techniques for non-contact vital sign detection," in *IEEE MTT-S Int. Microw. Symp. Dig.*, Jun. 2008, pp. 567–570, doi: 10.1109/MWSYM.2008.4633229.

[24] Y. Kinugasa, T. Saramaki, Y. Itoh, N. Sasaoka, K. Shiogai, and M. Kobayshi, "Modified subband adaptive notch filters for eliminating multiple sinusoids with reduced bias and faster convergence," in *Proc. IEEE Int. Symp. Circuits Syst. (ISCAS)*, May 2017, pp. 1–4, doi: 10.1109/ISCAS.2017.8050871.

[25] S. Haykin, *Adaptive Filter Theory*, 3rd ed. Upper Saddle River, NJ, USA: Prentice-Hall, 1996.
[26] T. C. Hsia and S. Sugimoto, "An investigation of adjustment gain design in stationary and nonstationary LMS adaptive algorithms," *IFAC Proc. Volumes*, vol. 15, no. 4, pp. 1335–1340, 1982, doi: 10.1016/S1474-6670(17)63183-5.
[27] T. Hsia, "Convergence analysis of LMS and NLMS adaptive algorithms," in *Proc. IEEE Int. Conf. Acoust., Speech, Signal Process.*, Apr. 1983, pp. 667–670, doi: 10.1109/ICASSP.1983.1172047.

MOUSHUMI TAZEN (Student Member, IEEE) received the B.E. degree in computer science and engineering from Northern University Bangladesh, in 2015, and the M.E. degree from the Department of Engineering, Graduate School of Sustainability Science, Tottori University, Japan, in 2021. Her research interest includes digital signal processing.

NAOTO SASAOKA (Member, IEEE) received the B.E., M.E., and Ph.D. degrees in electrical and electronic engineering from Tottori University, Japan, in 2002, 2004, and 2006, respectively. He is currently a Professor with the Graduate School of Engineering, Tottori University. His research interest includes digital signal processing.

YOSHIHARU OKAMOTO received the B.E., M.S., and Ph.D. degrees from Hokkaido University, Sapporo, Japan, in 1983, 1985, and 1993, respectively. He is currently the Director of the Veterinary Advanced Medical Research Institute, Wolves Hand Company Ltd., Osaka, Japan. His research interests include front-line cancer therapy, ozone therapy, and the development of biomonitors for animals.